J. Am. Soc. Mass Spectrom. (2015) 26:1938–1949
DOI: 10.1007/s13361-015-1218-7

RESEARCH ARTICLE

Competing Noncovalent Host-guest Interactions and H/D Exchange: Reactions of Benzyloxycarbonyl-Proline Glycine Dipeptide Variants with ND_3

Mahsan Miladi, Abayomi D. Olaitan, Behrooz Zekavat, Touradj Solouki

Department of Chemistry and Biochemistry, Baylor University, Waco, TX 76706, USA

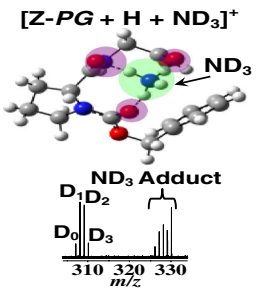

Abstract. A combination of density functional theory calculations, hydrogen/deuterium exchange (HDX) reactions, ion mobility-mass spectrometry, and isotope labeling tandem mass spectrometry was used to study gas-phase "host–guest" type interactions of a benzyloxycarbonyl (Z)-capped proline (P) glycine (G) model dipeptide (i.e., Z-PG) and its various structural analogues with ND_3. It is shown that in a solvent-free environment, structural differences between protonated and alkali metal ion (Na^+, K^+, or Cs^+)-complexed species of Z-PG affect ND_3 adduct formation. Specifically, $[Z\text{-}PG + H]^+$ and $[Z\text{-}PG\text{-}OCH_3 + H]^+$ formed gas-phase ND_3 adducts ($[Z\text{-}PG$ (or $Z\text{-}PG\text{-}OCH_3) + H + ND_3]^+$) but no ND_3 adducts were observed for $[Z\text{-}PG$ + alkali metal$]^+$ or $[Z\text{-}PG + H - CO_2]^+$. Experimentally measured and theoretically calculated collision cross sections (CCSs) of protonated and alkali metal ion-complexed Z-PG species showed similar trends that agreed with the observed structural differences from molecular modeling results. Moreover, results from theoretical ND_3 affinity calculations were consistent with experimental HDX observations, indicating a more stable ND_3 adduct for $[Z\text{-}PG + H]^+$ compared to [Z-PG + alkali metal]$^+$ species. Molecular modeling and experimental MS results for $[Z\text{-}PG + H]^+$ and [Z-PG + alkali metal]$^+$ suggest that optimized cation–π and hydrogen bonding interactions of carbonyl groups in final products are important for ND_3 adduct formation.

Keywords: Ion mobility, Host-guest, H/D exchange, Adduct formation, Ion-molecule reactions

Received: 11 February 2015/Revised: 26 May 2015/Accepted: 17 June 2015/Published Online: 21 August 2015

Introduction

The study of "host–guest" chemistry provides important insights for understanding chemical interactions involved in molecular recognition (e.g., designing drug delivery systems [1] and enzymes [2], sensor development [3, 4], and biological activities [5]). Gas-phase chemistry allows the study of important noncovalent interactions in a solvent-free environment [6–11]. For example, gas-phase studies provide details about the effects of noncovalent interactions, such as hydrogen bonding and metal ion complexation, on conformations of macromolecules [12–16].

Gas-phase hydrogen/deuterium exchange (HDX) mass spectrometry (MS) has been used extensively for structural/conformational studies of proteins/peptides [17–20] and their metal-complexed counterparts [21, 22]. Both HDX patterns and extent of deuterium uptake (or exchange of labile hydrogens) by protonated and metal-complexed proteins/peptides are used for structural elucidations [22–25]. However, the presence of possible competing reaction channels (such as gas-phase reagent adduct formation) [26, 27] may complicate the interpretation of the intended HDX reactions.

Although the mechanism(s) of gas-phase HDX reactions has been studied extensively [17, 18, 28–30], details of potential reagent adduct formations have not been adequately explored. For instance, it is not clear when and how the formation of a reagent adduct (e.g., $[peptide + nH + ND_3]^{n+}$, where "n" is the number of protons) competes with the anticipated HDX reactions. Deciphering possible mechanisms of these competing reactions is crucial to: (1) fill an important knowledge gap in host–guest chemistry, (2) enhance our ability to explore structure–function relationships, and (3) avoid misinterpretation of HDX data.

The present study was inspired by our previously observed deuterated ammonia (ND_3) adduct formation (e.g., with a Ca^{2+}-complexed "non-cyclic" host peptide [31]) and a recent HDX finding that suggested the formation of ND_3 adducts to be

Electronic supplementary material The online version of this article (doi:10.1007/s13361-015-1218-7) contains supplementary material, which is available to authorized users.

Correspondence to: Touradj Solouki; *e-mail:* Touradj_Solouki@baylor.edu

limited to "macrocyclic" peptide fragment ions [26]. Based on the observed adduct formation reactions (of cyclic and metal-complexed noncyclic peptides) and previous HDX reports [22, 31], we believe that metal ions play important roles in altering available HDX reaction channels and ND_3 adduct formations.

Using experimental MS and ion mobility spectrometry data and molecular modeling, we studied two aspects of gas-phase adduct formation: (1) effects of host molecules' structural variations on formation of stable gas-phase adducts, and (2) possibility of using host–guest interactions as probes for determining structural "compactness" of gas-phase ions.

We studied HDX reactions of protonated and alkali metal (Na^+, K^+, and Cs^+)-complexed species of a model dipeptide to uncover structural characteristics responsible for gas-phase HDX adduct formation in peptides. We selected a model dipeptide (and it's analogues) that contained a glycine (G) and a proline (P) with N-terminal benzyloxycarbonyl (Z) group (i.e., Z-PG, Scheme 1). Propensity for metal complexation and adduct formation, appropriate size (i.e., *m/z* values for reactant and product ions), and having a suitable structure with limited number of labile hydrogens were among the criteria for selecting Z-PG as a model peptide. Metal-complexed Z-PG species were used as model "compact" structures (as opposed to a "linear" type structure for protonated Z-PG) to study the role of structural compactness as a driving force for formation of gas-phase ND_3 adducts. In the context of data presented here, we refer to model dipeptides as "host" and ND_3 as "guest" partners.

Detailed experimental results from gas-phase HDX reactions and ion mobility-mass spectrometry (IM-MS) measurements for $[Z\text{-PG} + H]^+$, $[Z\text{-PG} + \text{alkali metal}]^+$, and $[Z\text{-PG} + H - CO_2]^+$ suggest that the formation of ammonia adducts with Z-PG species is structural/conformational-dependent. We also provide evidence from molecular modeling of protonated and alkali metal-complexed species of Z-PG that support our experimental observations. Ion mobility data and MS/MS results from collision-induced dissociation (CID) of isotopically labeled [Z-PG ($^{13}C_2$,^{15}N) + H]$^+$ (where "G" denotes an isotopically labeled glycine residue with two ^{13}C and one ^{15}N) reveal the importance of N-terminal Z carboxylic group in $[Z\text{-PG} + H]^+$ for ND_3 adduct formation. Based on the theoretically calculated Gibbs free energies for ND_3 adduct formation reactions, it is possible to predict which peptide structures can participate in host–guest interactions and form stable ND_3 adducts.

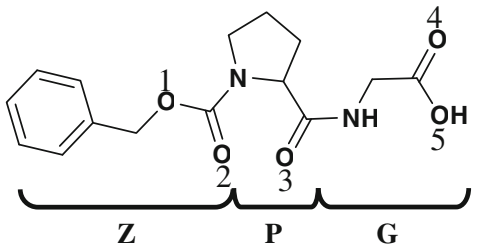

Scheme 1. Benzyloxycarbonyl (Z)-proline (P) glycine (G). Numbers denote positions of oxygen atoms in Z-PG

Experimental

Sample Preparation

Benzyloxycarbonyl-proline glycine (Z-PG), cesium chloride (CsCl), deuterated ammonia (ND_3), polypropylene glycol (PPG), and potassium chloride (KCl), were purchased from Sigma (Sigma-Aldrich, St. Louis, MO, USA). Z-PG-OCH_3 was synthesized by Peptide 2.0 (Peptide 2.0 Inc., Chantilly, VA, USA). Isotopically labeled Z-PG (where "G" denotes a glycine residue with two ^{13}C and one ^{15}N) was synthesized by Pierce Biotechnology (part of Thermo Fisher Scientific Inc., Waltham, MA, USA). Optima grade acetic acid, methanol, and water were purchased from Fisher Scientific (part of Thermo Fisher Scientific Inc., Waltham, MA, USA). All chemical reagents were used without further purification. Micromolar concentrations of peptide samples in electrospray solvent [methanol:water:acetic acid (49.95:49.95:0.1)] were used for electrospray ionization (ESI)-MS experiments. The original/commercially purchased peptide samples contained sodium (Na^+) and calcium (Ca^{2+}) ions and there was no need for addition of NaCl to Z-PG solutions to form sodium-complexed species of the dipeptides. However, millimolar concentrations of CsCl and KCl solutions were added to micromolar solutions of Z-PG to form potassium- and cesium-complexed species. Appropriate sample volumes were used to keep the final molar ratio of Z-PG:salt at 1:10.

$[Z\text{-PG} + K]^+$ (*m/z* 345.0847) and $[Z\text{-PG} + Ca - H]^+$ (*m/z* 345.0758) were differentiated based on resolving the two peaks and mass measurement accuracy values better than 2 ppm (which was possible in both Fourier transform-ion cyclotron resonance (FT-ICR) MS and IM-MS experiments presented here). Additionally, potassium- and calcium-complexed species of Z-PG could be differentiated based on their different collision cross section (CCS) values in IM-MS experiments (Supporting Information, Figure S1).

FT-ICR MS All gas-phase HDX mass spectrometry data were acquired using an IonSpec (former IonSpec Corp.—now a division of Agilent Technologies, Inc., Santa Clara, CA, USA) FT-ICR mass spectrometer equipped with an open-ended cylindrical Penning trap and a 9.4 tesla superconducting magnet (Cryomagnetics Inc., Oak Ridge, TN, USA). An Analytica ESI source (Analytica of Branford Inc., Branford, CT, USA) equipped with an in-house built spraying setup was used for ESI experiments [22]. A Harvard PHD 2000 syringe pump (Harvard Apparatus, Holliston, MA, USA) was used for direct infusion ESI. ESI flow rate was set to 0.3 μL min^{-1}. ESI voltage was set to +3 kV. Sustained off-resonance irradiation (SORI)-CID [32] was used for ion fragmentation in the ICR cell. Nitrogen gas (N_2) was used as the collision gas in SORI-CID experiments.

Prior to gas-phase HDX reactions, lowest mass most abundant isotopes [i.e., first carbon 12 isotopic peaks (or $^{12}C_{all}$ peaks, abbreviated as "D_0")] of protonated and metal-complexed Z-PG species were isolated in the ICR cell using a stored waveform inverse Fourier transform (SWIFT) technique [33]. To keep the relevant experimental conditions (e.g., ND_3 pressure and ICR cell temperature) identical, we simultaneously isolated the single isotopes of protonated and metal-complexed species of Z-PG to conduct HDX reactions. A pulsed-leak valve setup was used for ND_3 introduction [34]. Using the "pulsed-leak" valve setup, stable ND_3 pressures (inside the vacuum chamber) could be achieved in <1 s. Recorded ND_3 pressures were from direct readouts of a Granville-Phillips (Helix Technology Corp., Longmont, CO, USA) dual ion gauge controller (using series 274 Bayard-Alpert type ionization gauge tube outputs). All reported pressures for HDX reactions were corrected for (1) geometry factor [35], (2) magnetic field effect [36], and (3) sensitivity factor [37] according to a previously reported procedure [36].

IM-MS IM-MS experiments were conducted using a Waters Synapt G2-S HDMS (Waters Corp. Manchester, UK) system equipped with an orthogonal acceleration time-of-flight (oa-TOF) mass spectrometer operated in high resolution "W" mode (MassLynx 4.0, Waters Corp. Manchester, UK). For experiments presented here, it was important to use the "high resolution" mode (i.e., $m/\Delta m_{50\%} > 40{,}000$ at *m/z* 300) of the Synapt G2-S to differentiate between $[Z\text{-PG} + K]^+$ and $[Z\text{-PG} + Ca - H]^+$ species. The ESI flow rate and voltage were set to 0.3 μL min^{-1} and +3 kV, respectively. Both sampling cone and source offset voltages were set to +25 V. N_2 (~2.8 Torr) and argon (Ar) (~1.4×10^{-2} Torr) gases were used as buffer and collision gases, respectively. Helium (He) cell pressure was ~1.0×10^3 Torr. For experiments involving CID, ion populations of interest were isolated in the quadrupole mass filter prior to IM separation. Subsequently, *m/z*-isolated species were fragmented in either trap (pre-IM/CID) or transfer (post-IM/CID) cells.

We used a previously reported procedure by Ruotolo et al. [38] to obtain the experimental CCS values for protonated and alkali metal-complexed species of Z-PG. Sodium adduct species of PPG [39] were used as calibrants for CCS calculations. To obtain the CCS values of protonated and alkali metal-complex Z-PG species, the peak arrival times (ATs) of both calibrants and analytes (i.e., $[Z\text{-PG} + H]^+$ and $[Z\text{-PG} + \text{alkali metal}]^+$) were recorded at a constant wave height of +35 V and wide range of wave velocities (i.e., 800 m s^{-1}, 900 m s^{-1}, 1000 m s^{-1}, 1100 m s^{-1}, 1200 m s^{-1}). All IM measurements were repeated in triplicate; the reported CCSs are averages of 15 trials (three trials for each wave velocity) at the 95% confidence level.

Molecular Modeling Molecular mechanics MMX force field in PCModel 9.3 package (Serena Software, Bloomington, IN, USA) was used to search the conformational spaces of $[Z\text{-PG} + H]^+$ and $[Z\text{-PG} + H + ND_3]^+$ and protonated Z-PG mutants (Table 2). The 105 most stable structures (within 3 kcal mol^{-1} of the lowest energy structures) were selected for further optimization using MMX force field and simulated annealing at 298 and 1000 K. Similar energy conformers were obtained at both examined temperatures (i.e., 298 and 1000 K) for simulated annealing. For each analyte, the resulting low energy conformer was further optimized using B3LYP density functional theory (DFT) method [40]. Both $[Z\text{-PG} + H]^+$ and $[Z\text{-PG} + H + ND_3]^+$ structures were subsequently optimized at B3LYP/3-21G level and then at B3LYP/6-31+G(d,p) level (Gaussian 09 software: Gaussian Inc., Wallingford, CT, USA) [41]. Previous studies have suggested that B3LYP/3-21G and B3LYP/6-31+G(d,p) levels of theory provide excellent predictions for geometry optimizations and single-point energy calculations of protonated and metal-complexed species of peptides [42–45].

To optimize the geometries of alkali metal (Na^+, K^+, and Cs^+)-complexed Z-PG species, the proton in the PCModel optimized geometry of protonated Z-PG was replaced with an alkali metal cation (e.g., Na^+, K^+, or Cs^+) [22]. Subsequently, the structures of $[Z\text{-PG} + Na]^+$ and $[Z\text{-PG} + K]^+$ were optimized at B3LYP/3-21G and then at the B3LYP/6-31+G(d,p) levels. The geometry of $[Z\text{-PG} + Cs]^+$ was optimized using SDD pseudopotential basis set [46]. No imaginary frequencies were found for the optimized structures indicating that the optimized structures were not at their transition states.

Theoretical CCS Calculations CCSs of the optimized geometries of protonated and alkali metal-complexed species of Z-PG (obtained from DFT calculations) were calculated using a FORTRAN program ("Sigma") provided by Dr. Wyttenbach of the University of California at Santa Barbara. Ion-size scaled Lennard-Jones (LJ) model implemented in Sigma was used for CCS calculations [47, 48]. Temperature and CCS calculation accuracy in Sigma were set to 298 K and 2%, respectively.

Results and Discussion

HDX of $[Z\text{-PG} + H]^+$ and $[Z\text{-PG} + \text{Alkali Metal}]^+$

In this section, we present MS results from HDX reactions of protonated Z-PG and its alkali metal ion (Na^+, K^+, and Cs^+)-complexed counterparts with ND_3. Observed divergent host–guest chemical reactions between different Z-PG variants and ND_3 provide important details about hosts' interaction sites.

The selected model dipeptide, Z-PG, offers a number of advantages to carry out the intended experiments because (1) its C-terminal G residue is conformationally the least restricted amino acid [49]; hence, dipeptide's flexibility can allow formation of different metal complexes [22] (in contrast, proline's 5-membered ring connecting the side chain locks its dihedral angle at ~ –60° [50] constraining the structural variations of the selected Z-PG to regions near glycine), (2) it is sufficiently small to perform high-level DFT calculations and accurately estimate experimental and theoretical CCSs for $[Z\text{-PG} + H]^+$

and [Z-PG + alkali metal]$^+$ species, (3) protonated Z-PG contains a manageable number of exchangeable labile hydrogens (only three) to simplify HDX data interpretation, and (4) the Z group in Z-PG protects its N-terminus from forming "cyclic"-type structures [51, 52] and increases the molecular weight of the Z-PG dipeptide to 306 Da (which is above the low mass cut-off limit for external ion transfer of our 9.4 tesla ESI/FT-ICR mass spectrometer [53]). Additionally, the structural analogues of Z-PG (i.e., Z-GP, Z-PG-OCH_3, and isotopically labeled Z-PG) were commercially available; these Z-PG structural variants were necessary to identify the functional groups engaged in gas-phase ND_3 adduct formation of Z-PG.

Figure 1 shows the ESI/FT-ICR mass spectra of *m/z*-isolated protonated and alkali metal-complexed species of Z-PG after 5 s (top panels) and 600 s (bottom panels) HDX reaction times with ND_3 (pressure of 4.4×10^{-8} Torr).

After 5 s HDX reaction time with ND_3, the ESI/FT-ICR mass spectrum of [Z-PG + H]$^+$ (Figure 1a, top) shows the presence of both deuterium uptake and ND_3 adduct products (peak cluster labeled with roman numbers in Figure 1a, top). Based on an estimated ion-molecule collision frequency [54] of ~1.0 collision/s at $P_{ND3} \approx 4.4 \times 10^{-8}$ Torr (using ND_3 polarizability of $\alpha_{ND3} = 1.7$ Å^3) [36], HDX reaction between [Z-PG + H]$^+$ and ND_3 proceeds at near-collision rate [54]. Possibility of HDX reactions involving more than one H/D exchange per collision has been reported previously [17], which may explain the high rate of HDX for [Z-PG + H]$^+$ [exchange of all three available labile hydrogens of [Z-PG + H]$^+$ in only 5 s (Figure 1a, top)]. The observed near collision rate HDX for the reaction between [Z-PG + H]$^+$ and ND_3 might also be explained by considering the (1) consumption of D_0 ion population in two parallel reactions including "normal" HDX and ND_3 adduct formation, and (2) formation of long-lived gas-phase ND_3 adducts, which could increase the probability of deuterium transfer from ND_3 to [Z-PG + H]$^+$; subsequent dissociation of [Z-PG + H + ND_3]$^+$ and its deuterated ion population (in the time scale of FT-ICR measurements) can contribute to the observed HDX rate of [Z-PG + H]$^+$ species. However, formation of stable ND_3 adducts may preclude direct characterization of the precursor peptide ions in conventional gas-phase studies that aim to measure the number of HDX sites or kinetics of HDX reactions.

Under an identical number of gas-phase ion-molecule collisions, alkali metal-complexed (Na^+, K^+, or Cs^+) species of Z-PG did not form any ND_3 adducts (Figures 1c and d) and only showed deuterium uptake (Figure 1b to d) with reduced numbers of deuterium exchanges (e.g., only one compared with up to three for [Z-PG + H]$^+$). For instance, as shown in Figure 1a (top), the peak cluster at *m/z* range of 327 to 330 contains signals for ND_3 adduct of [Z-PG + H]$^+$; protonated Z-PG has three labile hydrogens and both [Z-PG + H]$^+$ and [Z-PG + H + ND_3]$^+$ exchange up to three of their labile hydrogens (i.e., peaks labeled as "D_3" and "V" in Figure 1a). In contrast, [Z-PG + Na]$^+$, [Z-PG + K]$^+$, and [Z-PG + Cs]$^+$ species show

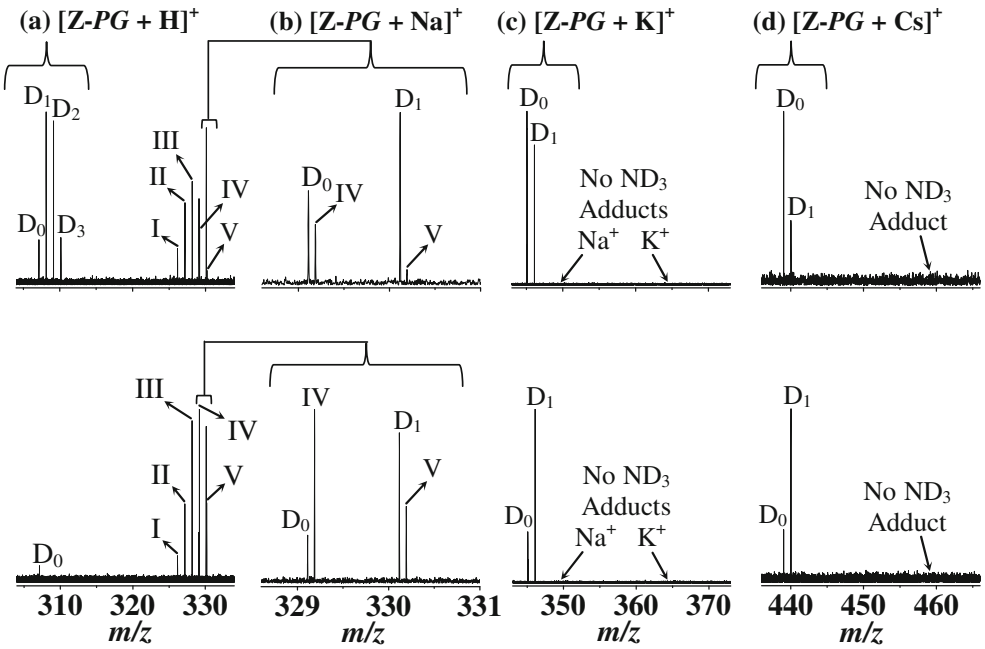

Figure 1. Expanded view ESI/FT-ICR mass spectra of SWIFT-isolated D_0 ion populations of [Z-PG + H]$^+$, [Z-PG + Na]$^+$, [Z-PG + K]$^+$, and [Z-PG + Cs]$^+$ after 5 s (top) and 600 s (bottom) HDX reaction time with ND_3 (at $P_{ND3} \approx 4.4 \times 10^{-8}$ Torr). D_n ($n = 0$ to 3) denotes the number of deuterium atom(s) incorporated in each of the Z-PG species. Roman numerals on top of the peaks in (**a**) and (**b**) designate the identities of ND_3 adduct species of [Z-PG + H]$^+$: I ≡ [D_0 + ND_2H]$^+$ (*m/z* 326); II ≡ [D_0 + ND_3]$^+$ (*m/z* 327); III ≡ [D_1 + ND_3]$^+$ (*m/z* 328); IV ≡ [D_2 + ND_3]$^+$ (*m/z* 329); V ≡ [D_3 + ND_3]$^+$ (*m/z* 330, fully exchanged ND_3 adduct). Arrows in (**c**) and (**d**) point to the expected *m/z* values for ND_3 adducts of [Z-PG + Na]$^+$ (panel c), [Z-PG + K]$^+$ (panel c), and [Z-PG + Cs]$^+$ (panel d) (which were not observed in these HDX experiments)

only one deuterium uptake (for each) out of their two available labile hydrogens. Observation of the ND_3 adducts of Z-PG at both ~1 s (data not shown) and 600 s (Figure 1, bottom) HDX reaction times (under identical ND_3 pressure of 4.4×10^{-8} Torr) suggests that collisional cooling does not enhance stability of the adduct products significantly. Species corresponding to competing HDX reaction channels (i.e., product ions labeled as peak "I" at *m/z* 326, and labeled as $[D_0 + ND_2H]^+$ where $D_0 \equiv [\text{Z-PG} + H]^+$) are also observed in the region showing ND_3 adducts of protonated Z-PG (Figure 1a, top and bottom). The following two reaction channels can yield the competing HDX products observed in Figure 1a: $[D_0 + ND_3]^+ + H_2O$ (residual background neutral water molecules present in the vacuum chamber) → $[D_0 + ND_2H]^+ + DHO$ and/or $[D_0]^+ + ND_2H$ (impurities present in ND_3 neutral reagent) → $[D_0 + ND_2H]^+$.

It has been suggested that similarity between gas-phase basicities (GBs) of the collision partners in HDX may favor the formation of gas-phase adducts [27]. Although, the GB similarity of host and guest partners may play a role in formation of stable gas-phase adducts, GB similarity is not "the key factor" for gas-phase reagent adduct formation. For instance, theoretically calculated GBs for ND_3 (~198 kcal mol^{-1}) and non-zwitterionic structure $[\text{Z-PG} + H]^+$ (~209 kcal mol^{-1}) are not similar; however, experimental HDX MS data show the presence of $[\text{Z-PG} + H + ND_3]^+$.

Observation of adduct formation in HDX reactions of non-cyclic $[\text{Z-PG} + H]^+$ with ND_3 indicates that in contrast to an earlier suggestion [26], gas-phase adduct formation may not be a suitable probe to differentiate between "linear"- and "macrocyclic"-type structures (i.e., both "linear" and "cyclic" ions tend to form ND_3 adducts). Therefore, other structural characteristics might be important for formation of stable host–guest interactions.

The observed smaller numbers of deuterium uptakes for $[\text{Z-PG} + \text{alkali metal}]^+$ (Figure 1b to d, top) compared with $[\text{Z-PG} + H]^+$ (Figure 1a, top) imply that alkali metal-complexed species of Z-PG adopt more compact structures (i.e., their labile hydrogens are more "protected") than their original protonated counterparts. This inference about size variations of protonated and alkali metal complexes of Z-PG (viz., for Na^+ and K^+) is consistent with experimentally measured CCSs from IM-MS data and molecular modeling results (both discussed in the following sections). Therefore, structural compactness is not the only determining factor for gas-phase reagent adduct formation; in other words, other structural factors (e.g., functional group orientation and availability) must be involved in stabilizing gas-phase ND_3 adducts.

It is worth noting that reaction trends for formation of the gas-phase ND_3 adducts of Z-PG and Z-GP (i.e., a Z-capped dipeptide with reverse amino acid sequence compared with Z-PG) were similar. For instance, similar to Z-PG, HDX reaction of protonated Z-GP with ND_3 also produced ND_3 adducts. Also, similar to Z-PG, no ND_3 adducts were formed with $[\text{Z-GP} + \text{Na, or K, or Cs}]^+$ species (Supporting Information, Figure S2). Experimental data and theoretical calculations presented in the following sections were designed to identify pertinent functional groups in Z-PG species involved in gas-phase adduct formation.

Theoretically Optimized Geometries of $[\text{Z-PG} + H]^+$ and $[\text{Z-PG} + \text{Alkali Metal}]^+$

To study the mechanism of neutral reagent adduct formation with $[\text{Z-PG} + H]^+$ upon HDX reaction, and to better interpret the HDX mass spectral patterns in Figure 1, we used DFT calculations and optimized the three-dimensional (3D) geometries of protonated Z-PG and its alkali metal-complexed and ND_3 adduct counterparts. Figure 2 shows the lowest energy 3D geometries of $[\text{Z-PG} + H]^+$ (panel a), $[\text{Z-PG} + Na]^+$ (panel b), $[\text{Z-PG} + K]^+$ (panel c), $[\text{Z-PG} + Cs]^+$ (panel d), and $[\text{Z-PG} + H + ND_3]^+$ (panel e). For all of the Z-PG species in Figure 2, their respective charge-solvated structures [55] were the most stable (lowest energy) geometries.

Theoretically optimized geometries in Figure 2 show a significantly different conformation for protonated Z-PG and its alkali metal-complexed species. For instance, as shown in Figure 2a, $[\text{Z-PG} + H]^+$ adopts an open conformation and its C-terminus is not involved in hydrogen bonding. In contrast, alkali metal-complexed species of Z-PG adopt compact conformations and carbonyl oxygen (O) atoms of glycine and proline residues and Z group ester-type O atom are involved in alkali metal complexation (Figure 2b to d). Observations from molecular modeling in Figure 2 (i.e., presence of more open conformation for $[\text{Z-PG} + H]^+$ compared with $[\text{Z-PG} + \text{alkali metal}]^+$) are consistent with the HDX data presented in Figure 1 (top panels) [i.e., occurrence of a larger number of deuterium uptake for $[\text{Z-PG} + H]^+$ (Figure 1a, top) compared with $[\text{Z-PG} + \text{alkali metal}]^+$ (Figure 1b to d, top)].

These observations are consistent with the previous reports that suggested the presence of a multi-dentate interactions [22] between alkali metal ions and peptides [22, 55–57]. Optimized geometries in Figure 2 show a tighter complexation for $[\text{Z-PG} + Na]^+$ than $[\text{Z-PG} + K]^+$ and $[\text{Z-PG} + Cs]^+$ as is evident from shorter coordination bond distances (d_1 to d_3 in Figure 2b to d) between Z-PG carbonyl oxygen atoms and Na^+ in $[\text{Z-PG} + Na]^+$. Figure 2e shows the 3D geometry of the most stable candidate structure for $[\text{Z-PG} + H + ND_3]^+$ in which three "host" carbonyl oxygen atoms (from P and G amino acids and Z group) are involved in hydrogen bonding with D atoms of "guest" ND_3.

At the first glance, it would seem that the Z carboxylic group, proline carbonyl oxygen, and C-terminal glycine carboxylic group are responsible for stabilizing $[\text{Z-PG} + H + ND_3]^+$ as these functional groups are involved in metal complexation in $[\text{Z-PG} + \text{alkali metal}]^+$ (Figure 2b to d). For example, as shown in Figure 2e, availability of these three acceptor carbonyl oxygen atoms maximizes the number and effectiveness (d_1, d_2, and $d_3 <$ 1.9 Å) of hydrogen bonds with ND_3. However, as discussed in the upcoming sections, our experimental MS data and theoretical calculations suggest that ND_3 adduct formation of Z-PG species depends on Z-PG conformational

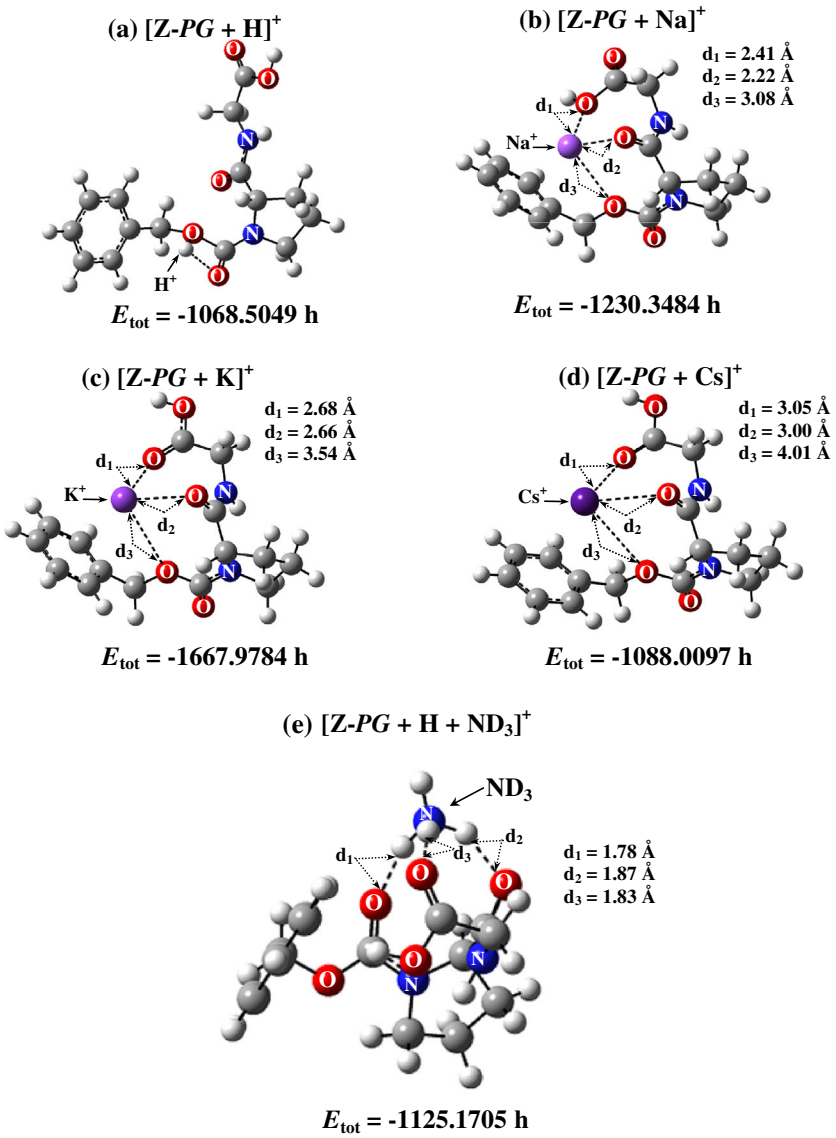

Figure 2. Optimized geometries of (**a**) [Z-PG + H]$^+$, (**b**) [Z-PG + Na]$^+$, (**c**) [Z-PG + K]$^+$, (**d**) [Z-PG + Cs]$^+$, and (**e**) [Z-PG + H + ND_3]$^+$. Carbon and hydrogen atoms are shown in dark grey and light grey colors, respectively. Nitrogen (in blue) and oxygen (in red) atoms are labeled as "N" and "O", respectively. Total energy (E_{tot}) for each structure is provided in Hartree (h). Sum of the electronic and thermal free energies for Z-PG, Na^+, K^+, Cs^+, and ND_3 are included in Table S1

changes, which result in stabilization of the final ND_3 adduct products.

IM-MS of [Z-PG + H]$^+$ and [Z-PG + Alkali Metal]$^+$

We used IM-MS to measure CCSs of protonated and alkali metal-complexed species of Z-PG. Experimentally obtained CCSs were correlated with the optimized 3D geometries from molecular modeling (Figure 2).

The IM profiles of each of the [Z-PG + H]$^+$, [Z-PG + Na]$^+$, [Z-PG + K]$^+$, and [Z-PG + Cs]$^+$ species (acquired using a Synapt G2-S HDMS system) showed a Gaussian-like AT distribution (data not shown), suggesting the presence of a single set of conformations for each species [22, 58]. We also used a previously reported post-IM/CID-chemometric approach to examine the presence of potential IM overlapped conformers [59]. Results from post-IM/CID-chemometric studies further confirmed the absence of resolvable multiple IM overlapped conformers for any of the protonated Z-PG and [Z-PG + alkali metal]$^+$ species. The peak AT values of all Z-PG species, under the IM experimental conditions described in the Experimental section, are provided in Table 1, second column. For meaningful comparisons, we converted the measured ion mobility ATs to CCSs (Table 1) using a previously reported procedure [38] (see Experimental section for more details).

Table 1, third column, contains a summary of the experimentally measured average CCS values for protonated and alkali metal-complexed Z-PG species. Based on the IM data, the following increasing order was observed for CCSs of Z-PG species: [Z-PG + Na]$^+$< [Z-PG + K]$^+$< [Z-PG + Cs]$^+$ ≈ [Z-PG + H]$^+$.

Table 1. Arrival Time Values, Experimental, and Theoretical Average Collision Cross Sections (CCSs), and Theoretically Calculated ND_3 Affinities of Z-PG Species

Z-PG Species	Arrival time (ms)[a]	Experimental CCS_{He} (Å^2)[b]	Theoretical CCS_{He} (Å^2)[b]	Theoretical ND_3 affinity (kcal mol^{-1})
$[Z\text{-PG} + H]^+$	05.90	120.84 (±0.73)	116.99 (±0.26)	+44.15
$[Z\text{-PG} + Na]^+$	05.35	113.23 (±0.48)	110.06 (±0.20)	+09.10
$[Z\text{-PG} + K]^+$	05.74	117.18 (±0.81)	112.92 (±0.17)	–01.99
$[Z\text{-PG} + Cs]^+$	06.04	120.72 (±0.48)	116.48 (±0.31)	+03.10

[a]Arrival time values were recorded using a wave velocity of 1000 m/s. Other IM parameters are given in the Experimental section
[b]Errors for CCS values at 95% confidence level (n = 15 for experimental and n = 40 for theoretical) are included in parentheses

These IM-MS results for CCS measurements are also consistent with the observed HDX mass spectral patterns in Figure 1 and suggest the presence of more compact structures for alkali metal-complexed species of Z-PG than their protonated counterpart. Experimentally measured CCSs in Table 1 suggest that smaller-size alkali metal ions bind tighter to Z-PG than larger size alkali metal ions. For instance, based on the experimental IM data, addition of Na^+ (r_{ion} = 0.97 Å) [60] to Z-PG reduces its average CCS by 6% (from ~120.84 Å^2 for $[Z\text{-PG} + H]^+$ to ~113.23 Å^2 for $[Z\text{-PG} + Na]^+$). Based on the calculated CCS values from multiple (n = 15) IM experiments, addition of Cs^+ (r_{ion} = 1.67 Å) [60] to Z-PG does not result in a statistically different average CCS value (at the 95% confidence level and using student's case II t-test for $n_1 = n_2 = 15$ = number of replicate IM measurements). However, molecular modeling results (Figures 2a and d) suggest that $[Z\text{-PG} + Cs]^+$ adopts a more compact structure than $[Z\text{-PG} + H]^+$ but the larger size of Cs^+ (r_{ion} = 1.67 Å) increases the overall CCS value of $[Z\text{-PG} + Cs]^+$.

We also compared the CCS values of protonated and alkali metal-complexed Z-PG species obtained from IM-MS measurements with those calculated from theoretically optimized candidate structures using DFT calculations. Table 1, fourth column, contains the theoretically calculated CCS values for Z-PG species. CCS values from 40 lowest energy optimized structures for each Z-PG species were used to calculate the theoretical average CCS values in Table 1 (column 4) (i.e., average of 40 CCS values for each Z-PG species).

The experimental and theoretical (Table 1, columns 3 and 4) CCSs of Z-PG species qualitatively agree with relative difference of <4%, consistent with the previously reported criterion for assigning structural geometries using IM [47]. Theoretical calculations also suggest similar (at the 95% confidence level) CCSs for $[Z\text{-PG} + H]^+$ and $[Z\text{-PG} + Cs]^+$. Experimental measurements and theoretical calculations of CCS are consistent and support the view that the addition of alkali metal ion introduces multi-dentate type bonding between alkali metals (viz., Na^+, K^+, and Cs^+) and the Z-PG dipeptide.

HDX and IM-MS of $[Z\text{-PG} + H - CO_2]^+$ Detailed inspection of the optimized structures in Figure 2 suggests that stable gas-phase ND_3 adduct formation with Z-PG species depends on the availability of backbone carbonyl groups from proline and glycine amino acids and benzyloxycarbonyl's ester group. To test this hypothesis, we conducted HDX experiments on $[Z\text{-PG} + H - CO_2]^+$ (*m/z* 263) generated from SORI-CID of *m/z*-isolated (D_0) $[Z\text{-PG} + H]^+$ (*m/z* 307) in the ICR cell.

Figure 3a shows the ESI/FT-ICR mass spectrum of $[Z\text{-PG} + H - CO_2]^+$ after ~600 s HDX reaction time with ND_3 (pressure ~4.4×10^{-8} Torr). Under identical experimental conditions as in Figure 1, bottom (e.g., number of ion-molecule collisions), $[Z\text{-PG} + H - CO_2]^+$ exchanged two of its three labile hydrogens with ND_3. However, unlike the $[Z\text{-PG} + H]^+$, which formed HDX reagent adducts, no ND_3 adduct was observed for $[Z\text{-PG} + H - CO_2]^+$ (Figure 3a).

Comparison of the HDX mass spectral results (from FT-ICR MS experiments) in Figures 1 bottom (panel a) and 3a suggests that loss of carboxylic group from $[Z\text{-PG} + H]^+$ makes the formation of ND_3 adduct with $[Z\text{-PG} + H]^+$ unfavorable. However, there are two possible positions for the loss of CO_2 from $[Z\text{-PG} + H]^+$: (i) carboxylic group from C-terminal glycine, or (ii) N-terminal benzyloxycarbonyl (Z) group (i.e., ester CO_2 in Scheme 1). Because both CO_2 loss products from pathways i and ii have identical *m/z* values (263.1390), MS alone cannot be used to distinguish them. Therefore, we attempted to use IM and CID to differentiate between the two CO_2 loss products of $[Z\text{-PG} + H]^+$.

Figure 3b shows the IM profile of *m/z*-isolated $[Z\text{-PG} + H - CO_2]^+$ generated from CID of $[Z\text{-PG} + H]^+$ in the Z-Spray ESI source of a Synapt G2-S. The bi-Gaussian IM

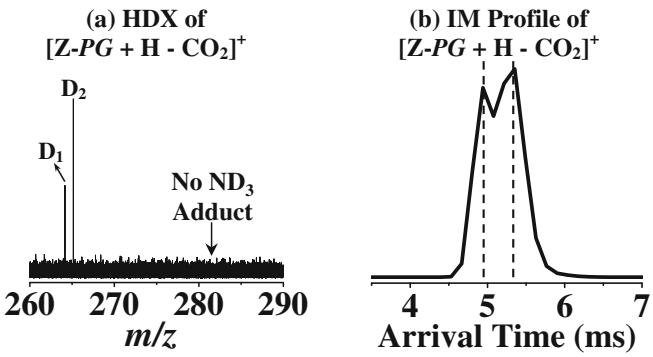

Figure 3. (**a**) ESI/FT-ICR mass spectrum of $[Z\text{-PG} + H - CO_2]^+$ after 600 s HDX reaction time with ND_3 (at $P_{ND3} \approx 4.4 \times 10^{-8}$ Torr). D_n (n = 1 and 2) denotes the number of deuterium atom(s) incorporated in $[Z\text{-PG} + H - CO_2]^+$. (b) Synapt G2-S ion mobility profile of $[Z\text{-PG} + H - CO_2]^+$. The two vertical dash lines in panel b show arrival time positions for the presumed two $[Z\text{-PG} + H - CO_2]^+$ conformers

profile peak shape in Figure 3b could be used to rationalize that neutral CO_2 is lost from both glycine and the Z group in $[Z\text{-}PG + H]^+$. However, it can also be hypothesized that $[Z\text{-}PG + H - CO_2]^+$ is the product of CO_2 loss from either glycine or Z group alone but adopts two different conformations/structures, which can be separated in IM cell. We were expecting to observe significantly different CID fragment ion types for the two IM overlapping $[Z\text{-}PG + H - CO_2]^+$ species. To test this hypothesis, we performed post-IM/CID MS experiments on $[Z\text{-}PG + H - CO_2]^+$. Although the IM profile for $[Z\text{-}PG + H - CO_2]^+$ showed two overlapping AT distributions (Figure 3b), their deconvoluted CID mass spectra (Supporting Information, Figure S3) showed identical fragment ions with notable differences in their relative abundances. These unexpected CID results for the two IM-overlapped $[Z\text{-}PG + H - CO_2]^+$ species suggested that CO_2 was indeed lost from a single site and prompted us to perform isotope labeling MS experiments to identify the site(s) of CO_2 losses.

Figure 4a shows the Synapt G2-S CID mass spectrum of isotopically labeled $[Z\text{-}P\underline{G} + H]^+$ (*m/z* 310). Underline in "G" is used to depict a C-terminal glycine that contains two ^{13}C and one ^{15}N isotopes. To acquire the CID mass spectrum in Figure 4a, isotopic envelope from *m/z* 310 to 311 (which included both major ($^{12}C_{13}{}^{13}C_2$ H_{19} O_5 N ^{15}N) and minor ($^{12}C_{12}$ $^{13}C_3$ H_{19} O_5 N ^{15}N) isotopes of $[Z\text{-}P\underline{G} + H]^+$) was mass-isolated. The isolated two isotopes at *m/z* 310 and 311 were subjected to CID in the Synapt G2-S trap cell by setting the potential difference between the trap cell exit and IM cell entrance to 14 V. If CO_2 could be lost from both C-terminal glycine and N-terminal Z group of $[Z\text{-}P\underline{G} + H]^+$, one would expect to observe two major peaks at *m/z* 265 ($[Z\text{-}P\underline{G} + H - {}^{13}CO_2]^+$) and 266 ($[Z\text{-}P\underline{G} + H - {}^{12}CO_2]^+$) in the CID mass spectrum of $[Z\text{-}P\underline{G} + H]^+$. However, as shown in Figure 4a, CID mass spectrum of $[Z\text{-}P\underline{G} + H]^+$ showed only the loss of $^{12}CO_2$ and no $^{13}CO_2$ loss (i.e., no fragment ion corresponding to $[Z\text{-}P\underline{G} + H - {}^{13}CO_2]^+$) was observed at *m/z* 265. Figure 4b shows the IM profile of $[Z\text{-}P\underline{G} + H - CO_2]^+$. Consistent with the view that the original CO_2 loss from Z-PG was from a single site and similar to the IM profile for $[Z\text{-}PG + H - CO_2]^+$ (Figure 3b), two ion populations were observed for $[Z\text{-}P\underline{G} + H - CO_2]^+$ (Figure 4b). Combination of the isotope labeling MS/MS, IMS, and HDX data confirmed that the observed CO_2 loss in Z-PG was indeed from the internal carboxylic group of benzyloxycarbonyl (Z) and not the carboxylic end of glycine. Hence, experimental findings were consistent with the theoretically predicted host–guest interaction sites in the optimized structure of $[Z\text{-}PG + H + ND_3]^+$ shown in Figure 2e. The absence of stable ND_3 adduct with $[Z\text{-}PG + H - CO_2]^+$ (in Figure 3a) is explained by loss of interaction between ND_3 and carbonyl functional group of Z-PG benzyloxycarbonyl (Z).

HDX of $[Z\text{-}PG\text{-}OCH_3 + H]^+$ C-terminal glycine amino acid in Z-PG contains both carbonyl and hydroxyl oxygen atoms; either or both functional groups could be involved in ND_3 adduct formation. To determine whether the presence of glycine hydroxyl group is important for Z-PG gas-phase adduct formation or not, we conducted HDX reactions on *m/z*-isolated species of $[Z\text{-}PG\text{-}OCH_3 + H]^+$ (*m/z* 321). In Z-PG-OCH_3, carbonyl from G is still available to participate in a host–guest type interaction but the hydrogen atom attached to glycine hydroxyl group (–O**H**) is replaced with a CH_3 group, which can interrupt the hydrogen bonding between ND_3 and glycine hydroxyl group in Z-PG.

Figure 5 shows the ESI/FT-ICR mass spectrum of protonated and metal-complexed Z-PG-OCH_3 species after 600 s HDX reaction time with ND_3 (pressure ~4.4×10^{-8} Torr). Similar to $[Z\text{-}PG + H]^+$ (Figure 1a, bottom), HDX mass spectrum of $[Z\text{-}PG\text{-}OCH_3 + H]^+$ showed the presence of both deuterium uptake and ND_3 adducts. Mass spectrum in Figure 5 (left panel) shows the presence of one deuterium uptake in $[Z\text{-}PG\text{-}OCH_3 + H]^+$ (peak labeled as D_1 in Figure 5) and up to one deuterium uptake in $[Z\text{-}PG\text{-}OCH_3 + H + ND_3]^+$ (peak

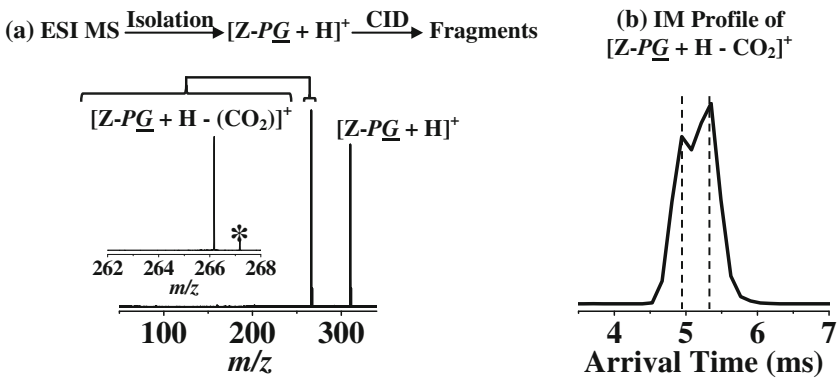

Figure 4. Synapt G2-S data for (**a**) CID mass spectrum of *m/z*-isolated $[Z\text{-}P\underline{G} + H]^+$ [isotopic distribution range from *m/z* 310 ($^{12}C_{13}$ $^{13}C_2$ H_{19} O_5 N ^{15}N) to *m/z* 311 ($^{12}C_{12}$ $^{13}C_3$ H_{19} O_5 N ^{15}N)], and (**b**) IM profile of $[Z\text{-}P\underline{G} + H - CO_2]^+$. "G" in Z-PG contains two labeled carbon 13 ($^{13}C_2$) isotopes and one labeled nitrogen fifteen ($^{15}N_1$) isotope. Inset in panel a shows the expanded view of *m/z* range between 262 to 268 (encompassing the *m/z* range for loss of carbon dioxide from $[Z\text{-}P\underline{G} + H]^+$). Peak at *m/z* 267 (labeled with star symbol "*") in panel a inset corresponds to natural ^{13}C isotope of $[Z\text{-}P\underline{G} + H - (CO_2)]^+$. The two vertical dash lines in panel b show arrival time positions for the presumed two $[Z\text{-}P\underline{G} + H - CO_2]^+$ conformers

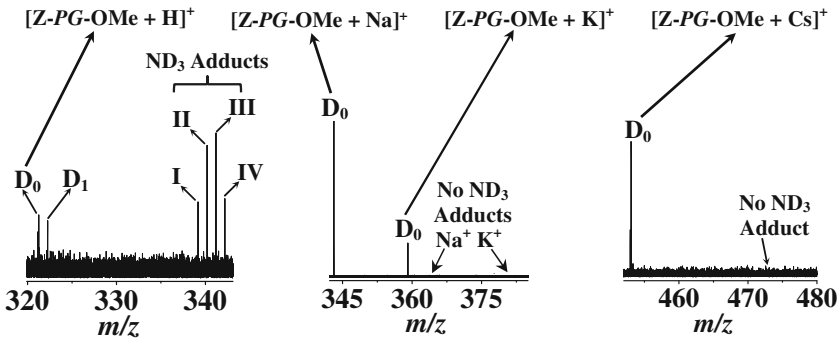

Figure 5. ESI/FT-ICR mass spectra of *m/z*-isolated (D_0) (left) [Z-PG-OMe + H]$^+$, (middle) [Z-PG-OMe + Na]$^+$, (middle) [Z-PG-OMe + K]$^+$, and (right) [Z-PG-OMe + Cs]$^+$ after 600 s reaction time with ND_3 (at $P_{ND3} \approx 4.4 \times 10^{-8}$ Torr). I ≡ $[D_0 + NDH_2]^+$ (*m/z* 339); II ≡ $[D_0 + ND_2H]^+$ (*m/z* 340); III ≡ $[D_0 + ND_3]^+$ (*m/z* 341); IV ≡ $[D_1 + ND_3]^+$ (*m/z* 342)

labeled as "IV" in Figure 5, left panel). No ND_3 adduct was observed for alkali metal (Na^+, K^+, and Cs^+)-complexed species of Z-PG-OCH_3 (Figure 5, middle and right panels).

Results in Figure 5 suggest that C-terminal glycine hydroxyl group is not involved in ND_3 adduct formation with Z-PG. HDX results in Figure 5 are consistent with the molecular modeling data in Figure 2e, suggesting that the O atom from glycine's carbonyl group is engaged in hydrogen bonding with ND_3.

Theoretical ND_3 Affinities of Z-PG Species Experimental and theoretical results discussed in previous sections suggest that the presence of all three Z-PG carbonyl groups is necessary for ND_3 adduct formation. The presence or absence of these carbonyl groups may influence ND_3 affinity of Z-PG species. To further explain the observed differences in ND_3 adduct formation of Z-PG species, we calculated ND_3 affinities of $[Z\text{-}PG + H]^+$ and $[Z\text{-}PG + \text{alkali metal}]^+$. The adduct formation of Z-PG species can be described by the following reaction:

$$[Z\text{–}PG + X]^+(g) + ND_3(g) \rightarrow [Z\text{–}PG + X + ND_3]^+(g)$$
$$X = H^+,\ Na^+,\ K^+,\ \text{or}\ Cs^+$$

(Reaction 1)

where "g" denotes a gas-phase species. Change in standard Gibbs free energy (ΔG) of reaction 1 was calculated according to Equation 1:

$$\Delta G_{298} = \sum (\varepsilon_0 + G_{corr})_{product} - \sum (\varepsilon_0 + G_{corr})_{reactants}$$

(Equation 1)

where "ΔG_{298}" denotes the change in standard Gibbs free energy of Reaction 1 at 298 K and "$(\varepsilon_0 + G_{corr})$" denotes sum of the electronic (ε_0) and corrected (for temperature of 298 K) thermal free energies. Values of $(\varepsilon_0 + G_{corr})$ (Table S1) were directly extracted from Gaussian 09 [41] output files of the reactants and products with optimized geometries (see Molecular Modeling section). In here (and Tables 1 and 2), negatives of the calculated "ΔG_{298}" values (i.e., -ΔG_{298}) for the reaction of Z-PG species with ND_3 are referred to as "ND_3 affinity" values.

Table 1, column 5, contains the calculated ND_3 affinities (in kcal mol^{-1}) for each of the Z-PG species. Comparison of ND_3 affinities of Z-PG species in Table 1 suggests that $[Z\text{-}PG + H]^+$ has the highest affinity (+44.15 kcal mol^{-1}) to form ND_3 adducts (as compared to any of the $[Z\text{-}PG + \text{alkali metal}]^+$ species). Calculated ND_3 affinities in Table 1 (column 5) are consistent with the experimental observations in Figure 1, suggesting the presence of stable ND_3 adducts for $[Z\text{-}PG + H]^+$. Moreover, as a predictive model, theoretically calculated ND_3 affinities for $[Z\text{-}PG + H]^+$ and $[Z\text{-}GP + H]^+$ suggest that ND_3 adduct formation for $[Z\text{-}PG + H]^+$ should be more favorable ($\Delta\Delta G_{298} \sim -16$ kcal mol^{-1}). Experimental results from 25 s HDX reaction time with ND_3 confirmed this theoretical prediction; for example, the observed ratio of (Σadducts/Σprotonated dipeptide) was 14.7 and 2.5 for $[Z\text{-}PG + H]^+$ and $[Z\text{-}GP + H]^+$, respectively (Supporting Information, Figure S4). Theoretically calculated ND_3 affinities in Table 1 suggest that adduct formations of $[Z\text{-}PG + Na]^+$ (ND_3 affinity, +09.10 kcal mol^{-1}) and $[Z\text{-}PG + Cs]^+$ (ND_3 affinity, +03.10 kcal mol^{-1}) with ND_3 are thermodynamically possible. However, neither $[Z\text{-}PG + Na + ND_3]^+$ nor $[Z\text{-}PG + Cs + ND_3]^+$ are observed (presumably dissociate to lose their guest ND_3) in time scale of FT-ICR MS experiment.

We also conducted ab initio molecular modeling calculations (MP2, 6-31+G(d,p) basis set) for [Z-PG + H or alkali metal]$^+$ and [Z-PG + H or alkali metal + ND_3]$^+$. Theoretically calculated ND_3 affinities of Z-PG species using ab initio were thermodynamically higher than ND_3 affinities obtained using DFT (Table 1, column 5). For example, theoretically calculated ND_3 affinities of $[Z\text{-}PG + H]^+$, $[Z\text{-}PG + Na]^+$, and $[Z\text{-}PG + K]^+$ from ab initio were +58.22 kcal mol^{-1}, +19.70 kcal mol^{-1}, and +7.66 kcal mol^{-1}, respectively. Nevertheless, these higher-level theoretical calculations revealed a similar trend for ND_3 affinities of Z-PG species (i.e., Table 1, ND_3 affinity of $[Z\text{-}PG + H]^+$ > ND_3 affinity of $[Z\text{-}PG + \text{alkali metal}]^+$).

Which Z-PG Functional Group(s) Are Important for Stable ND_3 Adduct Formation? Experimental and theoretical results presented in Figures 2, 3, and 4 show that Z group carbonyl O atom is among the important functional groups involved in

formation of stable ND_3 adducts with Z-PG. Additionally, data from molecular modeling in Figure 2 suggest that carbonyl groups from glycine and proline in $[Z\text{-}PG + H]^+$ are also involved in ND_3 adduct formation. Questions remain whether (1) the presence of proline and glycine carbonyl groups, and (2) remote cation–π interaction(s) with Z group phenyl ring in Z-PG, are important in stabilization of ND_3 adducts; if so, how significant are these interactions for stabilization of $[Z\text{-}PG + H + ND_3]^+$.

One approach for ranking the importance of Z-PG functional groups in ND_3 adduct formation is to synthesize Z-PG mutants in which Z-PG carbonyl oxygen atoms (or phenyl ring) are replaced with methyl (CH_3) groups (or cyclohexyl ring). Protonated species of Z-PG mutants can then be subjected to HDX reactions with ND_3 and the resulting HDX mass spectra can be inspected for the presence or absence of ND_3 adducts. Another approach is to use theoretical ND_3 affinities (similar to data presented in the previous section) of the Z-PG mutants and quantify the importance of a specific functional group in ND_3 adduct formation.

Here, we used the second approach and generated a set of Z-PG mutants in which we substituted carbonyl oxygen atoms and Z group phenyl ring with CH_3 and cyclohexane, respectively (Table 2, column 2). We then optimized 3D geometries of protonated Z-PG mutants and their corresponding ND_3 adducts. ND_3 affinities were calculated according to Reaction 1 and Equation 1. Methyl group with a van der Waals radius of ~1.7 Å (estimated from a van der Waals volume of 13.67 cm^3/mol) [61] has a comparable size to O atom (van der Waals radius of ~1.4 Å) [61]. Substitutions of carbonyl O atoms of Z-PG with CH_3 interrupt the hydrogen bonding interactions of ND_3 with carbonyl O (without a significant effect on steric hindrance).

Table 2 summarizes the theoretically calculated ND_3 affinities for various Z-PG mutants. Rows 1 to 3 in Table 2 contain ND_3 affinities for Z-PG mutants with one carbonyl O atom(s) replaced with CH_3 (numbers in O (2) to O (5) correspond to oxygen atom labeling indicated in Scheme 1). As a reference, Table 2 (row 4) also contains ND_3 affinity of a protonated Z-PG mutant in which all three carbonyl O atoms are replaced with CH_3. Row 5 of Table 2 contains ND_3 affinity of a protonated Z-PG mutant with its phenyl ring replaced with cyclohexyl ring. For comparison purposes, ΔND_3 affinities of Z-PG mutants {defined as ND_3 affinity (Mutant) – ND_3 affinity ($[Z\text{-}PG + H]^+$)} are also included in Table 2, column 4. A negative sign for ΔND_3 affinity indicates a less stable ND_3 adduct for mutant as compared with $[Z\text{-}PG + H]^+$ and vice versa.

Table 2. Theoretically Calculated ND_3 Affinities for Protonated Z-PG Mutants

Mutant number	Mutant type[a]	ND_3 affinity (kcal mol^{-1})	ΔND_3 affinity[b] (kcal mol^{-1})
1	O (2) → CH_3	+12.16	–31.99
2	O (3) → CH_3	+37.01	–07.14
3	O (4) → CH_3	+53.31	+09.16
4	O (2) → CH_3 O (3) → CH_3 O (4) → CH_3	–07.78	–51.93
5	Phenyl ring → cyclohexyl ring	+25.93	–18.22

[a]"x" numbers in O (x) refer to Z-PG oxygen numbers in Scheme 1
[b]ΔND_3 affinity = ND_3 affinity (Mutant) – ND_3 affinity ($[Z\text{-}PG + H]^+$)

Data in Table 2 suggest that all protonated Z-PG mutants form less stable ND_3 adduct products (compared with $[Z\text{-}PG + H]^+$), except for mutant 3 (i.e., substitution of glycine carbonyl O with CH_3). Among the three single O atom substitutions (mutants 1 to 3, Table 2), substitution of Z group carbonyl O atom with CH_3 (mutant 1 in Table 2) had the highest influence on reducing the stability of the Z-PG adducts (with ND_3). For example, substitution of Z group carbonyl O atom with CH_3 decreased the ND_3 affinity (Table 2, column 4) of protonated Z-PG by 31.99 kcal mol^{-1}. Reduction in theoretical ND_3 affinity of Z-PG mutant 1 (Table 2) (compared with $[Z\text{-}PG + H]^+$) is consistent with the absence of ND_3 adducts for $[Z\text{-}PG + H - CO_2]^+$ in Figure 4.

As expected, substitution of three Z-PG carbonyl O atoms with CH_3 (mutant 4 in Table 2) resulted in a thermodynamically unfavorable ND_3 adduct product (ND_3 affinity of –07.78 kcal mol^{-1}). Significant loss (by 51.93 kcal mol^{-1}) of ND_3 affinity for mutant 4 (compared with $[Z\text{-}PG + H]^+$) can be explained by interruption of favorable hydrogen bonding interactions of ND_3 with Z-PG carbonyl O atoms.

It has been shown that side chains of aromatic amino acids (e.g., phenylalanine, tyrosine, and tryptophan) contribute to stabilization of metal ion-complexed peptides through cation–π interactions [12, 62, 63]. Presence of Z group phenyl aromatic ring (cation–π interactions) may also contribute to the stabilization of "guest" (ND_3) and "host" (Z-PG) interactions. To evaluate the effect of π interactions on the formation of $[Z\text{-}PG + H + ND_3]^+$, we calculated ND_3 affinity for a Z-PG mutant in which the Z group phenyl ring in original Z-PG was replaced with cyclohexyl ring (i.e., mutant 5, Table 2). Theoretical ND_3 affinity of mutant 5 was +25.93 kcal mol^{-1} (i.e., 18.22 kcal mol^{-1} lower ND_3 affinity compared with $[Z\text{-}PG + H]^+$) suggesting that cation–π interactions play important roles in stabilization of the final $[Z\text{-}PG + H + ND_3]^+$ product.

Based on the experimental HDX data for Z-PG variants (e.g., Figures 1, 5, and S3) and theoretical ND_3 affinities provided in Table 1 (as well as ND_3 affinities of +27.92 kcal mol^{-1} and +28.15 kcal mol^{-1} for $[Z\text{-}PG\text{-}OCH_3 + H]^+$ and $[Z\text{-}GP + H]^+$, respectively), we predict the observation of ND_3 adduct for mutants 2, 3, and 5 (Table 2) in HDX reactions.

Conclusions

Theoretical and experimental approaches were used to investigate adduct formations in HDX reactions of protonated and metal-complexed Z-PG (and Z-GP) gas-phase ions with ND_3. Reactions of ND_3 with "linear" protonated Z-PG (and Z-GP) yielded gas-phase adducts but such adducts were not observed with "compact"

metal-complexed Z-PG and (Z-GP) species, presumably because of the unavailability of the functional groups necessary for host–guest interaction.

Formation of gas-phase reagent adducts with protonated Z-PG (and Z-GP) involved interactions between the guest neutral reagent and three carbonyl functional groups of the host dipeptide ions. Presented data suggest that previously reported ND_3 adducts of linear and cyclic peptide fragment ions [26, 31] may include a common host–guest interaction mechanism. In other words, ND_3 adduct formation can involve carbonyl groups of host cyclic [26] or linear [31] peptide ions. Examination of the host–guest chemistry in a solvent-free environment is important and may provide crucial details on functional groups governing solution-phase noncovalent interactions [2].

To the best of our knowledge, this is the first comprehensive study to examine gas-phase HDX reagent adduct formation by combining experimental (i.e., MS, IM-MS, and IM-MS/MS) and theoretical (i.e., molecular modeling and ND_3 affinity calculation) approaches.

Results presented here point to the importance of considering all competing gas-phase reaction channels during HDX of peptides (i.e., reagent adduct formation). Although the formation of gas-phase reagent adducts can complicate the interpretation of "normal" HDX uptake and reaction kinetics, it may also reveal important structural information such as orientation of peptides' backbone carbonyl groups.

Acknowledgments

Financial support from Baylor University and the Institute for Therapeutic Discovery is gratefully acknowledged. The authors thank Dr. Thomas Wyttenbach of the University of California, Santa Barbara for providing a copy of Sigma package, and Dr. Kevin L. Shuford of Baylor University for his valuable input on molecular modeling calculations. They also thank Paul Brown from Dr. Shuford's group for helping them with setting up a FORTRAN compiler for CCS calculations.

References

1. Hu, Q.D., Tang, G.P., Chu, P.K.: Cyclodextrin-based host–guest supramolecular nanoparticles for delivery: from design to applications. Acc. Chem. Res. **47**, 2017–2025 (2014)
2. Houk, K.N., Leach, A.G., Kim, S.P., Zhang, X.: Binding affinities of host–guest, protein–ligand, and protein–transition state complexes. Angew. Chem. Int. Ed. Engl. **42**, 4872–4897 (2003)
3. Zheng, J., Chen, C., Wang, X., Zhang, F., He, P.: A sequence-specific DNA sensor for Hepatitis B virus diagnostics based on the host–guest recognition. Sensors Actuators B **199**, 168–174 (2014)
4. Kriz, D., Ramström, O., Mosbach, K.: Molecular imprinting: new possibilities for sensor technology. Anal. Chem. **69**, 345A–349A (1997)
5. Boekhoven, J., Rubert Perez, C.M., Sur, S., Worthy, A., Stupp, S.I.: Dynamic display of bioactivity through host–guest chemistry. Angew. Chem. Int. Ed. Engl. **52**, 12077–12080 (2013)
6. Liou, C.-C., Brodbelt, J.S.: Comparison of gas-phase proton and ammonium ion affinities of crown ethers and related acyclic analogs. J. Am. Chem. Soc. **114**, 6761–6764 (1992)
7. Brodbelt, J.S.: Probing molecular recognition by mass spectrometry. Int. J. Mass Spectrom. **200**, 57–69 (2000)
8. Dearden, D.V., Liang, Y., Nicoll, J.B., Kellersberger, K.A.: Study of gas-phase molecular recognition using Fourier transform ion cyclotron resonance mass spectrometry (FTICR/MS). J. Mass Spectrom. **36**, 989–997 (2001)
9. Schalley, C.A., Verhaelen, C., Klarner, F.G., Hahn, U., Vogtle, F.: Gas-phase host–guest chemistry of dendritic viologens and molecular tweezers: a remarkably strong effect on dication stability. Angew. Chem. Int. Ed. Engl. **44**, 477–480 (2005)
10. Ko, J.Y., Heo, S.W., Lee, J.H., Oh, H.B., Kim, H., Kim, H.I.: Host–guest chemistry in the gas phase: complex formation with 18-crown-6 enhances helicity of alanine-based peptides. J. Phys. Chem. A **115**, 14215–14220 (2011)
11. Lee, T.C., Kalenius, E., Lazar, A.I., Assaf, K.I., Kuhnert, N., Grun, C.H., Janis, J., Scherman, O.A., Nau, W.M.: Chemistry inside molecular containers in the gas phase. Nat. Chem. **5**, 376–382 (2013)
12. Ryzhov, V., Dunbar, R.C., Cerda, B., Wesdemiotis, C.: Cation-pi effects in the complexation of Na^+ and K^+ with Phe, Tyr, and Trp in the gas phase. J. Am. Soc. Mass Spectrom. **11**, 1037–1046 (2000)
13. Zhu, M.M., Rempel, D.L., Zhao, J., Giblin, D.E., Gross, M.L.: Probing Ca^{2+}-induced conformational changes in porcine calmodulin by H/D exchange and ESI-MS: effect of cations and ionic strength. Biochemistry **42**, 15388–15397 (2003)
14. Rozman, M., Gaskell, S.J.: Noncovalent interactions of alkali metal cations with singly charged tryptic peptides. J. Mass Spectrom. **45**, 1409–1415 (2010)
15. Dunbar, R.C., Steill, J.D., Polfer, N.C., Oomens, J.: Metal cation binding to gas-phase penta-alanine: divalent ions restructure the complex. J. Phys. Chem. A **117**, 1094–1101 (2013)
16. Dunbar, R.C., Berdenb, G., Oomens, J.: How does a small peptide choose how to bind a metal ion? IRMPD and computational survey of CS versus Iminol binding preferences. Int. J. Mass Spectrom. **354/355**, 356–364 (2013)
17. Campbell, S., Rodgers, M.T., Marzluff, E.M., Beauchamp, J.L.: Deuterium exchange reactions as a probe of biomolecule structure. Fundamental studies of gas phase H/D exchange reactions of protonated glycine oligomers with D_2O, CD_3OD, CD_3CO_2D, and ND_3. J. Am. Chem. Soc. **117**, 12840–12854 (1995)
18. Green, M.K., Lebrilla, C.B.: Ion-molecule reactions as probes of gas-phase structures of peptides and proteins. Mass Spectrom. Rev. **16**, 53–71 (1997)
19. Polfer, N.C., Dunbar, R.C., Oomens, J.: Observation of zwitterion formation in the gas-phase H/D-exchange with CH_3OD: solution-phase structures in the gas phase. J. Am. Soc. Mass Spectrom. **18**, 512–516 (2007)
20. Rand, K.D., Pringle, S.D., Murphy III, J.P., Fadgen, K.E., Brown, J., Engen, J.R.: Gas-phase hydrogen/deuterium exchange in a traveling wave ion guide for the examination of protein conformations. Anal. Chem. **81**, 10019–10028 (2009)
21. Reyzer, M.L., Brodbelt, J.S.: Gas-phase H/D exchange reactions of polyamine complexes: $(M + H)^+$, $(M + \text{alkali metal})^+$, and $(M + 2H)^{2+}$. J. Am. Soc. Mass Spectrom. **11**, 711–721 (2000)
22. Solouki, T., Fort Jr., R.C., Alomary, A., Fattahi, A.: Gas-phase hydrogen-deuterium exchange reactions of a model peptide: FT-ICR and computational analyses of metal induced conformational mutations. J. Am. Soc. Mass Spectrom. **12**, 1272–1285 (2001)
23. Fattahi, A., Solouki, T.: Conformational analysis of metal complexed model peptides and their fragment ions using FT-ICR MS and gas-phase H/D exchange reactions. Proceedings of the 49th ASMS Conference on Mass Spectrometry and Allied Topics. Chicago, IL, 27–31 May 2001
24. Fattahi, A., Zekavat, B., Solouki, T.: H/D exchange kinetics: experimental evidence for formation of different b fragment ion conformers/isomers during the gas-phase peptide sequencing. J. Am. Soc. Mass Spectrom. **21**, 358–369 (2010)
25. Miladi, M., Zekavat, B., Munisamy, S.M., Solouki, T.: A systematic study on the effect of histidine position and fragment ion size on the formation of b_n ions. Int. J. Mass Spectrom. **316/318**, 164–173 (2012)
26. Somogyi, A., Harrison, A.G., Paizs, B.: Using gas-phase guest–host chemistry to probe the structures of b ions of peptides. J. Am. Soc. Mass Spectrom. **23**, 2055–2058 (2012)

27. Green-Church, K.B., Limbach, P.A., Freitas, M.A., Marshall, A.G.: Gas-phase hydrogen/deuterium exchange of positively charged mononucleotides by use of Fourier-transform ion cyclotron resonance mass spectrometry. J. Am. Soc. Mass Spectrom. **12**, 268–277 (2001)
28. Cox, H.A., Julian, R.R., Lee, S.W., Beauchamp, J.L.: Gas-phase H/D exchange of sodiated glycine oligomers with ND_3: exchange kinetics do not reflect parent ion structures. J. Am. Chem. Soc. **126**, 6485–6490 (2004)
29. Rozman, M.: The gas-phase H/D exchange mechanism of protonated amino acids. J. Am. Soc. Mass Spectrom. **16**, 1846–1852 (2005)
30. Rozman, M., Bertosa, B., Klasinc, L., Srzic, D.: Gas phase H/D exchange of sodiated amino acids: Why do we see zwitterions? J. Am. Soc. Mass Spectrom. **17**, 29–36 (2006)
31. Solouki, T., Fort, R., Alomary, A., Fattahi, A.: Gas-phase hydrogen-deuterium exchange reactions of model peptides: conformational analyses by FT-ICR. Proceedings of the 48th ASMS Conference on Mass Spectrometry and Allied Topics. Long Beach, CA, 11–15 June 2000
32. Gauthier, J.W., Trautman, T.R., Jacobson, D.B.: Sustained off-resonance irradiation for collision-activated dissociation involving Fourier transform mass spectrometry. collision-activated dissociation technique that emulates infrared multiphoton dissociation. Anal. Chim. Acta **246**, 211–225 (1991)
33. Wang, T.C., Ricca, T.L., Marshall, A.G.: Extension of dynamic range in Fourier transform ion cyclotron resonance mass spectrometry via stored waveform inverse Fourier transform excitation. Anal. Chem. **58**, 2935–2938 (1986)
34. Jiao, C.Q., Ranatunga, D.R., Vaughn, W.E., Freiser, B.S.: A pulsed-leak valve for use with ion trapping mass spectrometers. J. Am. Soc. Mass Spectrom. **7**, 118–122 (1996)
35. Solouki, T., Szulejko, J.E.: Bimolecular and unimolecular contributions to the disparate self-chemical ionizations of alpha-pinene and camphene isomers. J. Am. Soc. Mass Spectrom. **18**, 2026–2039 (2007)
36. Zekavat, B., Miladi, M., Alfdeilat, A., Somogyi, A., Solouki, T.: Evidence for sequence scrambling and divergent H/D exchange reactions of doubly-charged isobaric b type fragment ions. J. Am. Soc. Mass Spectrom. **25**, 226–236 (2014)
37. Bartmess, J.E., Georgiadis, R.M.: Empirical methods for determination of ionization gauge relative sensitivities for different gases. Vacuum **33**, 149–153 (1983)
38. Ruotolo, B.T., Benesch, J.L., Sandercock, A.M., Hyung, S.J., Robinson, C.V.: Ion mobility-mass spectrometry analysis of large protein complexes. Nat. Protoc. **3**, 1139–1152 (2008)
39. Gidden, J., Wyttenbach, T., Jackson, A.T., Scrivens, J.H., Bowers, M.T.: Gas-phase conformations of synthetic polymers: poly(ethylene glycol), poly(propylene glycol), and poly(tetramethylene glycol). J. Am. Chem. Soc. **122**, 4692–4699 (2000)
40. Becke, A.D.: Density-functional thermochemistry III. The role of exact exchange. J. Chem. Phys. **98**, 5648–5652 (1993)
41. Frisch, M.J., Trucks, G.W., Schlegel, H.B., Scuseria, G.E., Robb, M.A., Cheeseman, J.R., Scalmani, G., Barone, V., Mennucci, B., Petersson, G.A., Nakatsuji, H., Caricato, M., Li, X., Hratchian, H.P., Izmaylov, A.F., Bloino, J., Zheng, G., Sonnenberg, J.L., Hada, M., Ehara, M., Toyota, K., Fukuda, R., Hasegawa, J., Ishida, M., Nakajima, T., Honda, Y., Kitao, O., Nakai, H., Vreven, T., Montgomery Jr., J.A., Peralta, J.E., Ogliaro, F., Bearpark, M., Heyd, J.J., Brothers, E., Kudin, K.N., Staroverov, V.N., Kobayashi, R., Normand, J., Raghavachari, K., Rendell, A., Burant, J.C., Iyengar, S.S., Tomasi, J., Cossi, M., Rega, N., Millam, N.J., Klene, M., Knox, J.E., Cross, J.B., Bakken, V., Adamo, C., Jaramillo, J., Gomperts, R., Stratmann, R.E., Yazyev, O., Austin, A.J., Cammi, R., Pomelli, C., Ochterski, J.W., Martin, R.L., Morokuma, K., Zakrzewski, V.G., Voth, G.A., Salvador, P., Dannenberg, J.J., Dapprich, S., Daniels, A.D., Farkas, Ö., Foresman, J.B., Ortiz, J.V., Cioslowski, J., Fox, D.J.: Gaussian-09, Revision C.01. Gaussian, Inc, Wallingford (2010)
42. Aribi, H.E., Orlova, G., Rodriquez, C.F., Almeida, D.R.P., Hopkinson, A.C., Siu, K.W.M.: Fragmentation mechanisms of product ions from protonated tripeptides. J. Phys. Chem. B **108**, 18743–18749 (2004)
43. Polfer, N.C., Paizs, B., Snoek, L.C., Compagnon, I., Suhai, S., Meijer, G., von Helden, G., Oomens, J.: Infrared fingerprint spectroscopy and theoretical studies of potassium ion tagged amino acids and peptides in the gas phase. J. Am. Chem. Soc. **127**, 8571–8579 (2005)
44. Bythell, B.J., Csonka, I.P., Suhai, S., Barofsky, D.F., Paizs, B.: Gas-phase structure and fragmentation pathways of singly protonated peptides with N-terminal arginine. J. Phys. Chem. B **114**, 15092–15105 (2010)
45. Dunbar, R.C., Steill, J.D., Polfer, N.C., Oomens, J.: Metal cation binding to gas-phase penta-alanine: divalent ions restructure the complex. J. Phys. Chem. A **117**, 1094–1101 (2012)
46. Leininger, T., Nicklass, A., Kuchle, W., Stoll, H., Dolg, M., Bergner, A.: The accuracy of the pseudopotential approximation: non-frozen-core effects for spectroscopic constants of alkali fluorides XF (X = K, Rb, Cs). Chem. Phys. Lett. **255**, 274–280 (1996)
47. von Helden, G., Hsu, M.-T., Gotts, N., Bowers, M.T.: Carbon cluster cations with up to 84 atoms: structures, formation mechanism, and reactivity. J. Phys. Chem. **97**, 8182–8192 (1993)
48. Wyttenbach, T., von Helden, G., Batka Jr., J.J., Carlat, D., Bowers, M.T.: Effect of the long-range potential on ion mobility measurements. J. Am. Soc. Mass Spectrom. **8**, 275–282 (1997)
49. Ramachandran, G.N., Ramakrishnan, C., Sasisekharan, V.: Stereochemistry of polypeptide chain configurations. J. Mol. Biol. **7**, 95–99 (1963)
50. Ho, B.K., Coutsias, E.A., Seok, C., Dill, K.A.: The flexibility in the proline ring couples to the protein backbone. Protein Sci. **14**, 1011–1018 (2005)
51. Chin, W., Piuzzi, F., Dimicoli, I., Mons, M.: Probing the competition between secondary structures and local preferences in gas phase isolated peptide backbones. Phys. Chem. Chem. Phys. **8**, 1033–1048 (2006)
52. Harrison, A.G.: Cyclization of peptide b_9 ions. J. Am. Soc. Mass Spectrom. **20**, 2248–2253 (2009)
53. Zekavat, B., Szulejko, J.E., LaBrecque, D., Olaitan, A.D., Solouki, T.: Efficient injection of low mass ions into high magnetic field FTICR mass spectrometers. Rapid Commun. Mass Spectrom. **28**, 230–238 (2014)
54. Marshall, A.G., Hendrickson, C.L., Jackson, G.S.: Fourier transform ion cyclotron resonance mass spectrometry: a primer. Mass Spectrom. Rev. **17**, 1–35 (1998)
55. Dunbar, R.C., Steill, J.D., Polfer, N.C., Berden, G., Oomens, J.: Peptide bond tautomerization induced by divalent metal ions: characterization of the iminol configuration. Angew. Chem. Int. Ed. Engl. **51**, 4591–4593 (2012)
56. Dunbar, R.C., Oomens, J., Berden, G., Lau, J.K., Verkerk, U.H., Hopkinson, A.C., Siu, K.W.: Metal ion complexes with HisGly: comparison with PhePhe and PheGly. J. Phys. Chem. A **117**, 5335–5343 (2013)
57. Chen, L., Gao, Y.Q., Russell, D.H.: How alkali metal ion binding alters the conformation preferences of gramicidin a: a molecular dynamics and ion mobility study. J. Phys. Chem. A **116**, 689–696 (2012)
58. Zekavat, B., Miladi, M., Becker, C., Munisamy, S.M., Solouki, T.: Combined use of post-ion mobility/collision-induced dissociation and chemometrics for b fragment ion analysis. J. Am. Soc. Mass Spectrom. **24**, 1355–1365 (2013)
59. Zekavat, B., Solouki, T.: Chemometric data analysis for deconvolution of overlapped ion mobility profiles. J. Am. Soc. Mass Spectrom. **23**, 1873–1884 (2012)
60. Frensdorff, H.K.: Stability constants of cyclic polyether complexes with univalent cations. J. Am. Chem. Soc. **93**, 600–606 (1971)
61. Bondi, A.: Van der Waals volumes and radii. J. Phys. Chem. **68**, 441–451 (1964)
62. Ma, J.C., Dougherty, D.A.: The cation-p interaction. Chem. Rev. **97**, 1303–1324 (1997)
63. Dunbar, R.C.: Complexation of Na^+ and K^+ to aromatic amino acids: a density functional computational study of cation-p interactions. J. Phys. Chem. A **104**, 8067–8074 (2000)